World Academy of Science, Engineering and Technology
International Journal of Mechanical and Mechatronics Engineering
Vol:5, No:9, 2011

# Verification of K-ω SST Turbulence Model for Supersonic Internal Flows

J. Kolář, V. Dvořák



***Abstract*—**In this work, we try to find the best setting of Computational Fluid Dynamic solver available for the problems in the field of supersonic internal flows. We used the supersonic air-to-air ejector to represent the typical problem in focus. There are multiple oblique shock waves, shear layers, boundary layers and normal shock interacting in the supersonic ejector making this device typical in field of supersonic inner flows. Modeling of shocks in general is demanding on the physical model of fluid, because ordinary conservation equation does not conform to real conditions in the near-shock region as found in many works. From these reasons, we decided to take special care about solver setting in this article by means of experimental approach of color Schlieren pictures and pneumatic measurement. Fast pressure transducers were used to measure unsteady static pressure in regimes with normal shock in mixing chamber. Physical behavior of ejector in several regimes is discussed. Best choice of eddy-viscosity setting is discussed on the theoretical base. The final verification of the k-ω SST is done on the base of comparison between experiment and numerical results.

***Keywords*—**CFD simulations, color Schlieren, k-ω SST, supersonic flows, shock waves.

## I. Introduction

OPTIMIZATION of all types is becoming extremely attractive in these days. Improving of machines performance, design and cost are goals for nowadays engineers. Aerodynamic optimization is not outstanding from this trend, even though the handling with aerodynamic variables is not trivial. Generally, we need to get able to quantify product quality (cost, efficiency, strength, design quality) for every optimization process known. In other words, we need to be able establish and solve the objective. In aerodynamics, Computational Fluid Dynamic is the most widespread and comprehensive tool used to solve objective. Regrettably, despite modern codes, solvers and increased computational power the optimization employing CFD codes remains tricky. Commonly used gradient-optimum-search-based methods may found local or even global optimum, which vary from real optimum (within design space) due to the errors of the objective enumeration [1]-[4]. Few-percentage incorrectness of CFD results may affect the algorithm which gets strayed afterwards. Thus, the goal of this article is to find the best adjustment of CFD solver in field of supersonic inner aerodynamic of compressible fluid. Further, this solver setting is to be used for the consequent optimization process based on Micro Genetic Algorithm and Shape Similarity Query. We focused on one of the most demanding CFD problems, which is supersonic air-to-air ejector. There is a complex aerodynamic of subsonic, transonic and supersonic flows within. See Fig. 1 to clearly understand the operating of the two-dimensional ejector.

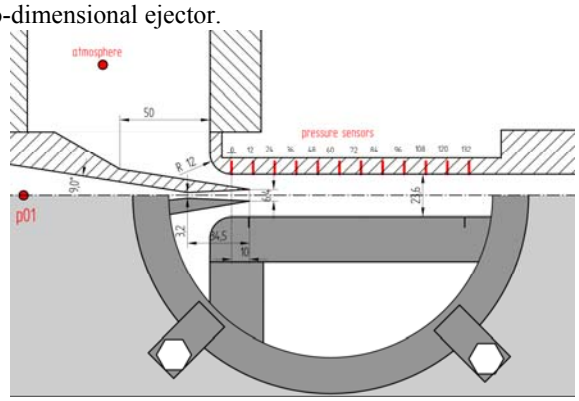


Fig. 1 Scheme of the supersonic air-to-air ejector.

The third dimension not included in the Fig. 1 is the ejector's depth set to 80 mm. Primary air compressed to $p_{01}$, which exceeds the critical isentropic pressure ratio in the throat defined as

$$\left({}^{p}/_{p_{01}}\right)_{is} < 0.528, \quad (1)$$

flows from the air supply to the primary nozzle in the middle left of the Fig. 1. Aerodynamic throat appears near the geometrical throat of the primary channel. Downstream, supersonic air velocity is induced in the diverging part of the nozzle. Isentropic Design Mach number given by section rate $\left({}^{A}/_{A_{crit}}\right)_{is} = 2$ was set to $M_{1,is} = 2.197$.After the supersonic air stream passes the trailing edge, viscosity and turbulence effects overwhelm secondary stream and the secondary flow is induced from the surrounding as shown by in [4]. As soon as the mass flow rate of the overwhelmed air gets big enough, the throat appears and secondary flow become supersonic downstream the throat. Design Mach number of secondary flow is $M_{2,is} = 1.609$ Velocity of the primary and secondary flows are given only by ejector geometry and vary one to the other than. Shear layer divides the regions of various flow speeds in vertical direction. Because of non-zero trailing edge angle, both streams must adapt stream in respect to the new direction. This course-adaption happens across oblique shock waves, being inclined by the angle defined by downstream Mach number as

$$\alpha = \pm \arcsin\left({}^{1}/_{M}\right). \quad (2)$$

Once the oblique shock wave is being induced it spreads towards the symmetry plane and ejector wall. Near the symmetry plane, the interaction of two oblique shocks takes

J. Kolář,F. is with the Technical University of Liberec, Department of Power Engineering, Faculty of Mechanical Engineering, Studentská 2, Liberec, 46017, Czech Republic (e-mail: jan.kolar1@tul.cz)
V. Dvořák is with the Technical University of Liberec, Department of Power Engineering, Faculty of Mechanical Engineering, Studentská 2, Liberec, 46017, Czech Republic (e-mail: vaclav.dvorak@tul.cz).

place. In the near-wall region the interaction with boundary layer causes separation of subsonic boundary layer and deflected reflection of the shock might by observed. Afterwards, wall-reflected-shock crosses the region of variable flow velocity called shear layer. Within this interaction originally straight shock is s-like deformed as shown in the reference [5], [6]. These interactions repeat many times thanks to the multiple reflections. Shock spreads downstream, than. As every shock causes the decrease of the stream Mach number, every subsequent shock weakens downstream until faded of. More detailed theoretic about supersonic flows may be found in the reference [7].The mathematically-physical capture of the shock by means of Finite Volume Methods (FVM) is very demanding. Real shock cross-dimension was established about 1E-6 m, which is rapidly different from ordinary size of element in FVM. Moreover, flow states variable and directions change shock-like across the wave. In conjunction with relative macro-scale of finite elements, the governing equations defined for FVM should not be valid in the near-shock regions. Further details may be found e.g. in [8]. The strongest form of the oblique shock is the normal shock. Even though flow direction remains the same across, state variables and Mach number rapidly changes from supersonic to subsonic. Although theoretical bases of normal shock and its position in channel are well established in e.g. [7], experimental and numerical investigation remains uncompleted. From these reasons, we decided to investigate the regimes of the ejector covering design regimes and regimes with normal shock within mixing chamber. These regimes are being one of the most demanding on CFD codes in general and on eddy-viscosity models especially [9]. Further, the influence of selected parameters of eddy viscosity in selected regimes is investigated.

## II. Methods of Experimental Investigation

We used two approaches to investigate the air flow within the ejector whose drawing is in the Fig.1. Two dimensional ejectors is made of aluminum alloy insets and Cr-Mo side plates making the ejector heavy and stable.

### *A. Pneumatic Measurement*

There are pressure-probe-holes drilled into the mixing chamber with diameter 0.5 mm. For position of drill holes see the top part of the Fig. 1. Probes are further connected to the fast pressure transducers, which works with the sample frequency 1000 Hz. DEWE analog-digital converter collect and transform data for DEWE-Soft on the supervising PC. All pressure data are stored in RAW form for further post-processing. Presented pressure values in steady state are averaged in the integral sense for the time interval 2 s. Presented unsteady pressure course are scaled-only with conserved sample rate.

### *B. Color Schlieren Photography*

Circular aperture made of optic glasses enables optical experiments on the ejector. See bottom part of the Fig. 1. Basically, Schlieren photography takes advantage of density change of the air. These changes may be visualized thanks to dependency of refraction index on medium density. Resulting bend of the light beam in gases then can be defined as

$$\Delta\alpha = -\frac{L}{n} K \frac{d\rho}{dy}. \quad (3)$$

Moreover, we use the circular four quadrant color filter to colorize the segment, where the light beams were bent to. The beam bend direction is given by the direction of density gradient. In our experiment we used the filter colorized to the blue (upper left), green (upper right), red (lower left), orange (lower right), seen in the direction of oncoming light beams. There is clear un-colorized spot in the middle of filter. This spot enables the unbent beams to remain uncolorized. Electric spot flash-light is used to produce sufficient light intensity. With that light intensity, we were able to set exposure time of capturing DLSR camera to 1/640 s. This enables take Schlieren pictures clear and bright enough.

## III. Methods of Numerical Investigation

The main scope of this article is to verify the flow field obtained by means of numerical simulations. We use ordinary Finite Volume Method to divide the two-dimensional domain into finite elements. Within the domain, governing equation completed by energy and state equations must comply to the boundary conditions. Unfortunately the system of differential equations is not fully closed. We do close this system by means of turbulence models. There is hierarchy of the turbulence models in the Fig. 2

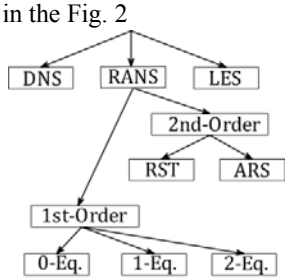


Fig. 2 Hierarchy of turbulence models.

Due to the high Reynolds number expected, Large Eddy Simulations would not be reasonable choice for supersonic flows. Thus, we use the Reynolds Averaged Navier-Stokes (RANS) equations. In order to be able to compute turbulent flows with the RANS equations it is necessary to develop turbulence models to predict the Reynolds stresses and the scalar transport terms and close the system of mean flow equations. We are forced to decrease overall size of finite volumes due to large gradients expected. Moreover, we expect large amount of runs of simulations when ejector is being optimized. Therefore we cannot accept computationally expensive choice of the $2^{nd}$ Order RANS. From the remaining choices of the $1^{st}$ Order RANS, 0-Equation (Mixing Length) and 1-Equation (Spalart-Allmaras) models usually do not capture turbulence effects. These effects can be very strong mainly in shear and boundary layers. The 2-Equations turbulence models are based on the Boussinesq hypothesis, saying that effects of turbulence may be modeled by increased

molecular viscosity by the value of turbulent viscosity. Resulting viscosity is defined as

$$\nu = \nu_M + \nu_T. \quad (4)$$

Various models were developed to model the turbulence viscosity $\nu_T$. Models based either on turbulence kinetic energy $k$ and dissipation $\varepsilon$ or specific dissipation rate ω have become of the most attractive. We focus on one of the most promising modification of $k-\omega$.:Shear Stress Transport (SST), whose modified turbulent viscosity formulation accounts for the transport effects of the principal turbulent shear stress. The promising is also gradual change of the SST from the standard $k-\omega$ in the inner region of the boundary layer to a high-Reynolds-number version of the $k-\varepsilon$ model in the outer part of the boundary layer.

### *A. Theoretical Analysis of k-ω SST turbulence model*

The turbulence kinetic energy k and the specific dissipation rate ω for SST modification of k-ω are obtained from the following transport equations [10]

$$\frac{\partial}{\partial t}(\rho k) + \frac{\partial}{\partial x_i}(\rho k u_i) = \frac{\partial}{\partial x_j}\left(\Gamma_k \frac{\partial k}{\partial x_j}\right) + \widetilde{G_k} - Y_k + S_k \text{ and} \quad (5)$$

$$\frac{\partial}{\partial t}(\rho \omega) + \frac{\partial}{\partial x_i}(\rho \omega u_i) = \frac{\partial}{\partial x_j}\left(\Gamma_k \frac{\partial \omega}{\partial x_j}\right) + G_\omega - Y_\omega + S_\omega + D_\omega . \quad (6)$$

In these equations $\widetilde{G_k}$ represents the production of turbulence kinetic energy due to mean velocity gradients, calculated as

$$\widetilde{G_k} = -\rho \overline{u'_i u'_j} \frac{\partial u_j}{\partial x_i} \quad \text{and} \quad (7)$$

$G_\omega$ represents the generation of ω, calculated as

$$G_\omega = \propto \frac{\omega}{k} G_k. \quad (8)$$

In the high-Reynolds-number form of the $k-\omega$ model

$$\alpha = \alpha_\infty = 1 . \quad (9)$$

Further in equations (1), $Y_k$ and represent the dissipation of k due to turbulence, calculated as

$$Y_k = \rho \beta^* f_{\beta^*} k, \text{ where} \quad (10)$$

$$f_{\beta^*} = 1. \quad (11)$$

Thus,

$$Y_k = \rho \beta^* k \omega, \text{ where} \quad (12)$$

$$\beta^* = \beta_i^* [1 + \varsigma^* F(M_t)], \text{ where} \quad (13)$$

$$\beta_i^* = \beta_\infty^* \left( \frac{\frac{4}{15} + \left(\frac{Re_t}{R_\beta}\right)^4}{1 + \left(\frac{Re_t}{R_\beta}\right)^4} \right) \quad (14)$$

In the high-Reynolds-number flows

$$\beta_i^* = \beta_\infty^* . \quad (15)$$

In the equation (13), $F(M_t)$ represents compressibility correction. This is important member as the supersonic flows must include compressibility effects. Compressibility correction is defined as

$$F(M_t) = \begin{cases} 0 & M_t \le M_{t0} \\ M_t^2 - M_{t0}^2 & M_t > M_{t0} \end{cases}, \text{ where} \quad (16)$$

$$M_t^2 = \frac{2k}{\kappa R T} \quad (17)$$

This yields, that in low-turbulent-kinetic-energy regions the compressibility correction is not applied. In supersonic flow we expect $M_t > M_{t0}$.The ω-dissipation term $Y_\omega$ in equation (6) is defined as

$$Y_\omega = \rho \beta f_\beta \omega^2, \text{ where} \quad (17)$$

$$f_\beta = 1. \quad (18)$$

Thus,

$$Y_\omega = \rho \beta \omega^2, \text{ where} \quad (19)$$

$$\beta_i = F_1 \beta_{i,1} + (1 - F_1)\beta_{i,2}, \text{ where} \quad (20)$$

$$F_1 = tanh(\Phi_1^4), \text{ where} \quad (21)$$

$$\Phi_1 = min\left[ max\left( \frac{\sqrt{k}}{0.09\omega y}, \frac{500\mu}{\varrho y^2 \omega} \right), \frac{4\rho k}{\sigma_{\omega,2} D_\omega^+ y^2} \right], \text{ where} \quad (22)$$

$$D_\omega^+ = \left[ 2\rho \frac{1}{\sigma_{\omega,2}} \frac{1}{\omega} \frac{\partial k}{\partial x_j} \frac{\partial \omega}{\partial x_j}, 10^{-10} \right]. \quad (23)$$

The SST $k-\omega$ model is based on both the standard $k-\omega$ model and standard $k-\epsilon$. To blend these models together, the standard $k-\epsilon$ model has been transformed into equations based on $k$ and $\omega$. This leads to the introduction of cross-diffusion term defined as

$$D_\omega = 2(1 - F_1)\varrho \sigma_{\omega,2} \frac{1}{\omega} \frac{\partial k}{\partial x_j} \frac{\partial \omega}{\partial x_j} \quad (24)$$

From the above analysis of $k-\omega$ SST model we can find model constants and their likely values in supersonic flows empirically established in past. These constants are summarized in the Table 1 [11].

TABLE I
*k − ω SST* MODEL CONSTANTS

| Symbols | Values | Symbols | Values |
|---|---|---|---|
| $\sigma_{k,1}$ | 1.176 | $\alpha_\infty$ | 1 |
| $\sigma_{\omega,1}$ | 2.0 | $\alpha_0$ | 1/9 |
| $\sigma_{k,2}$ | 1.0 | $\beta_\infty^*$ | 0.09 |
| $\sigma_{\omega,2}$ | 1.168 | $R_\beta$ | 8 |
| $a_1$ | 0.31 | $R_k$ | 6 |
| $\beta_{i,1}$ | 0.075 | $R_\omega$ | 2.95 |
| $\beta_{i,2}$ | 0.0828 | $\zeta^*$ | 1.5 |
| $\alpha_\infty^*$ | 1 | $M_{t0}$ | 0.25 |

These constants are to be in a focus of sensitivity analysis in future with the aim to clearly understand their influence on supersonic simulations.

### *B. Boundary Conditions and Solver Settings*

We used the commercial code FLUENT to solve 2D RANS equations with the $k-\omega$ SST by Finite Volume Technique.

For all equations, convective terms are discretized using a second-order upwind scheme; inviscid fluxes are derived using a second order flux splitting achieving the necessary upwinding and dissipation close to shocks. We choose the density based solver with the implicit formulation. Diffusion terms are always cast into a central difference form. The criterion for assessing convergence was based on the root mean square of the density residues expressed by

$$R(\xi) = \left[\sum_{i=1}^{M} \left(\frac{\partial \xi}{\partial t}\right)_i^2\right]^{1/2} \quad (25)$$

Where M is the number of grid points and ξ is the variable considered to check (mass, energy, momentum, etc.). Generally, computations are stopped when residuals fall below $1x10^{-6}$ and when the solution is was no longer changing. In addition, at convergence, the mass imbalance is checked on each inlet and outlet boundaries. All mentioned requirements were successfully meet in about 50 000 iteration steps with Courant-Friedrichs-Lewy (CFL) number set to 1 [11]. Boundary conditions were set to pressure inlet/outlet with non-reflecting boundary condition (outlet pressure at infinity). Turbulent intensity was set to 8 % at the primary nozzle inlet and to 2 % at the secondary nozzle intake. Both, gauge total pressure $p_{01}$ and the outlet gauge pressure $p_{exit}$ vary for every regimes mentioned. Symmetric computational domain split by the symmetry boundary condition consists of $4.5E^5$ quadrilateral elements with original mesh size 0.2 mm. We defined the grid-gradual boundary layer in ten levels from the size of $5E^{-3}$ mm in wall adjacent cells to the free stream value.

## IV. Results of Experiment

There are color Schlieren pictures taken in various regimes which differs in stagnation gauge pressure $p_{01}$ and stagnation gauge pressure at the ejector outlet $p_{exit}$. The first regime shown in the Fig. 3 is normal-shock-free. Multiple interactions and reflections of oblique shocks can be observed. Shear layer develops all the way downstream the mixing chamber. Among others, curved sonic line may be found near secondary throats.

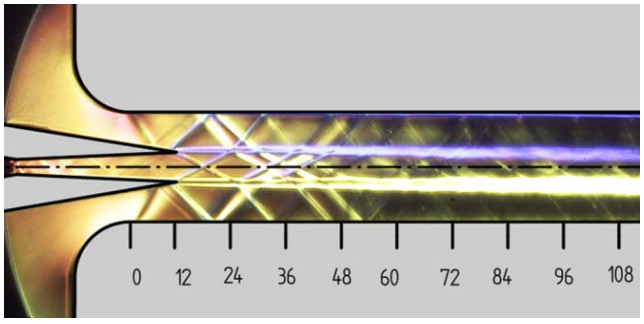


Fig. 3 Schlieren picture of the supersonic ejector in operation. Design regime. $p_{01} = 175$ kPa,. $p_{exit} = -77\ kPa$.

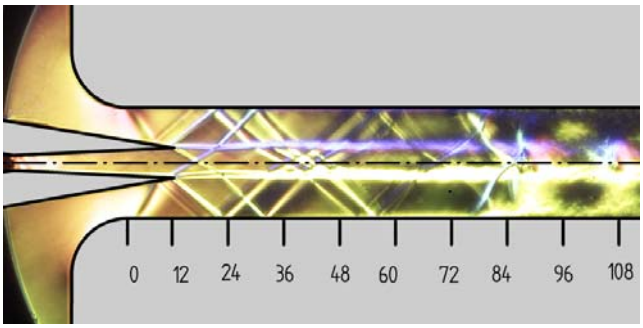


Fig. 4 Schlieren picture of the supersonic ejector in operation. Regime with the strong shock. $p_{01} = 111$ kPa,. $p_{exit} = -11\ kPa$

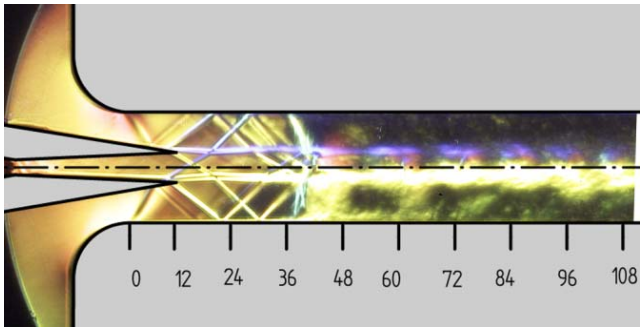


Fig. 5 Schlieren picture of the supersonic ejector in operation. Regime with the strong shock. $p_{01} = 107$ kPa,. $p_{exit} = -12.5\ kPa$

In the Fig. 3-5 we can observe a strong shock closing the field of oblique shock waves. Because of it, the strong shock is to be called closing chock. We can observe the upstream movement of closing shock with $p_{01}$ decreasing and $p_{exit}$ increasing. Closing shock is formed by separation of boundary layer, which underlies in subsonic part to the adverse pressure gradient. Even the weak oblique shock than can induce increment of adverse pressure gradient, which cause the boundary layer separation. Separated boundary layer is than forming the shape of supersonic region. Compression waves ordinate at the convex-shaped region. These waves further interact into strong shock. See Fig. 6.

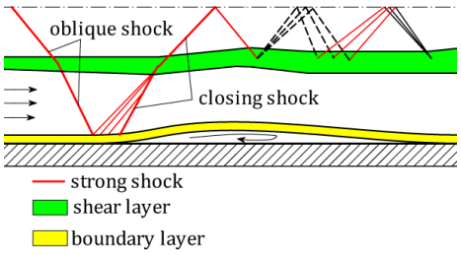


Fig. 6 Formation of closing shock

## V. Results of Numerical Simulations

There is a brief introduction into results obtained by means of numerical simulations in the Fig. 7. Contours of Mach number do not conform to the physical principle of density gradient

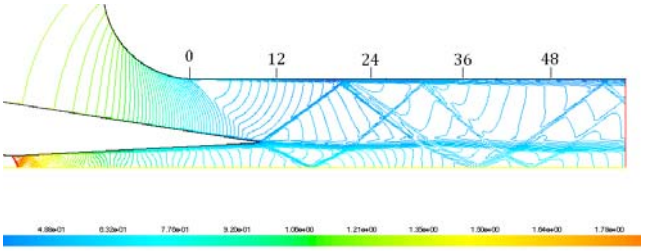


Fig. 7 Contours of density obtained by numerical simulation. Design regime

From the Fig.7 we can clearly see well modeled shock waves induced at the trailing edge. Nevertheless, modeled secondary flow reaches higher velocity as can be recognized from the inclination of shock waves. The inclination is defined by the relation (2). The x-coordinate of the deflection point than moves significantly downstream the chamber. The idea of the over-predicted secondary velocity conforms to the Fig. 8, where lower values of stagnation pressure are modeled all the way in mixing chamber.

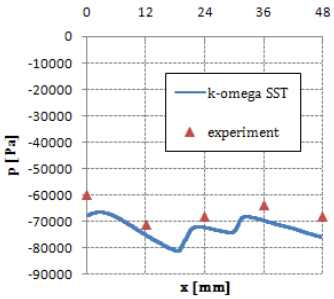


Fig. 8 Stagnation pressure at mixing chamber wall. Comparison of the experiment and numerical simulation

The inclination of shock in the primary stream seems to be conforming to the experiment. This leads to the conclusion of the over-predicted shear stress by $k-\omega$SST turbulence model with its standard coefficients.

## VI. Conclusions

Experimental measurement by mean of the Schlieren color pictures and pneumatic transducers were carried out on the supersonic air-to-air-ejector. Several pictures of flow field in various operating regimes are proposed. Brief theory-based analysis of closing shock is included. Thanks to that, we are able to predict expected problems for numerical simulations of the ejector. The theoretical analysis of the most promising turbulence viscosity model $k-\omega$SST is proposed and its model coefficients are reviewed. Complete setting of numerical simulation is presented. We have found good agreement of shock waves prediction and boundary layer separation, but shear stress between two streams is over-predicted. Consequently, the secondary air velocity reaches higher velocity then real. Recently, we work on sensitivity analysis of model constants to improve accuracy. Afterwards, test of modified constants is planned in remaining regimes with the closing shock in mixing chamber.

## Acknowledgement

Authors would like to thanks to the Czech Science Foundation which supported this work by grant no. P101/10/1709. This work was also supported by research plan MSN 4674788501 and SGS 2823.

## References

[1] Breitkopf, P. and Coelho, R. F. Multidisciplinary design optimization in computational mechanics: Wiley-ISTE, 2010. ISBN-10 1848211384.
[2] Hynek, J. Genetic algorithms and genetic programing (in Czech). Prague : Grada Publishing ,a. s., 2008. ISBN 978-80-247-2695-3.
[3] Dvořák, V. and Kolář, J. Shape optimization of supersonic ejectors with several primary nozzles. Lisboa, Portugal : In the 2nd International Conference on Engineering Optimization, 6.-9. september 2010. ISBN 978-989-96264-3-0.
[4] Dvořák, V. Shape optimization of supersonic ejector for supersonic wind tunnel. s.l. : In.: Applied and Computational Mechanics, 2010. pp. 15-24. ISSN 1802-680X.
[5] Kolář, J. and Šafařík, P. Interaction of oblique shock wave with shear layer. Plzeň : In Proceedings of the International Conference XXVII: Meeting of Departments of Fluid Mechanics and Thermomechanics, 2008. pp. 163-170. ISBN 978-80-7043-666-0.
[6] Moeckel, W. E. Interaction of oblique shock waves with regions of variable pressure, entropy and energy. Washington : NACA, 1952. TN 2725.
[7] Shapiro, A. H. The dynamics and thermodynamics of compressible fluid flow. New York : The Ronald Press Company, 1953. ISBN 0826080758.
8] Versteeg, H. K. and Malalasekera, W. An Introduction to Computational fluid dynamics, The Finite Volume Method: Pearson Education Limited 2007, ISBN 978-0-13-127498-3.
[9] Wilcox, D. Reassessment of the scale determining equation for advanced turbulent models. 1988. AIAA J. 26 (11),1299-1310.
[10] Menter, F. R. Two-equations Eddy-viscosity turbulence models for engineering applications. 1994. AIAA J. 32(8), 1598-1605.
[11] Inc., Fluent. Fluent user documentation. Lebanon : s.n., 2006.
from the biography.